Journal of Applied Sciences

ISSN 1812-5654

science alert

ANSInet
an open access publisher
http://ansinet.com

Journal of Applied Sciences 7 (22): 3400-3409, 2007
ISSN 1812-5654

Computer Aided Design and 3D Magnetostatic Analysis of a Permanent Magnet Spherical Motor

[1]Yusuf Öner and [2]Ahmet Altintas
[1]Department of Electrical and Electronics Engineering,
Pamukkale University, 20017 Kınıklı, Denizli, Turkey
[2]Faculty of Technical Education, Dumlupinar University,
Simav, Kutahya, Turkey

Abstract: In this study, the analysis and design of a dc version of spherical permanent magnet motor, which are capable of three degrees-of-freedom motion, have been introduced. The spherical permanent magnet rotor with 4-pole is made of NdFeB magnet slices. The bearing (or support mechanism), different from preceding, is made from a hollow semi-spherical teflon material. The validity of the analysis and design techniques are confirmed by numeric calculations and measurements taken from a prototype. Numeric analysis of the electro-mechanical forces is performed by a commercial software package (Ansoft Maxwell 3D) using FE method. The spherical motor in question is capable of ±45° pan-tilt movements in addition to spinning 360° continuously.

Key words: Spherical motor, 3DOF actuator, magneto-static analysis

INTRODUCTION

Many advanced manufacturing processes require smooth, high-precision and/or high-speed robotic manipulations in three dimensional space. Electrical motors, as energy conversion devices, are widely used in industrial applications. Various kinds of motors have been introduced up to date. All of those conventional motor are one degree-of-freedom (DOF) motors. One-DOF motors including stepper, switched-reluctance or servo motors have reached their maturity for a long time (Lee *et al*., 2004). While these motors can provide accurate motions in a single-axis, the combinations of these single-axis motors as multi-DOF devices are rather bulky and incapable; because three one-DOF motors, together with a relatively complicated and heavy transmission system, have to be used to deliver the required motion in the three axes. This arrangement inevitably compromises the dynamic performance and servo-tracking accuracy, due to the combined effects of inertia, backlash, non-linear friction and elastic deformation of gears. Multi-DOF motors can produce perfect solution to alleviate these problems.

A spherical motor, a multi-DOF motor, is capable of three-DOF motions within a single joint. Without cascading actuators or motors in series or parallel to achieve multi-DOF motion, workspace singularities and structural rigidity can be improved for better dynamic response. Spherical motor not only encompasses the above attributes but also due to its direct drive characteristics, bulky and inefficient gear reduction mechanism can be eliminated. This greatly enhances the performance and efficiency of this class of motor. The potential application can be found largely in robotics manipulator and positioning devices (Lim *et al*., 2005).

Spherical motors have been the subject of research for several decades. Spherical motors take a number of forms which include the induction motors (Davey *et al*., 1987; Foggia *et al*., 1988), the direct-current motors (Hollis and Ralph, 1989; Kaneko *et al*., 1989; Lim *et al*., 2004), the stepper motors (Lee and Kwan, 1991), the variable reluctance motors (Roth and Lee, 1995; Zhou and Lee, 1996) and the ultrasonic motors (Zhao *et al*., 2005; Shigeki *et al*., 1996). The three dimensional nature of the electromagnetic field distribution in almost all of the foregoing spherical motors make their electromagnetic and dynamic behavior difficult to analyze and this has been a significant obstacle to their design optimization and servo application. As a result, the potential benefits of employing spherical motors have not been realized. Therefore, most of these motor forms remain un-commercialized.

Corresponding Author: Yusuf Öner, Department of Electrical and Electronics Engineering, Pamukkale University, 20017 Kınıklı, Denizli, Turkey Tel: +90 258 213 4030 Fax: +90 258 212 5538

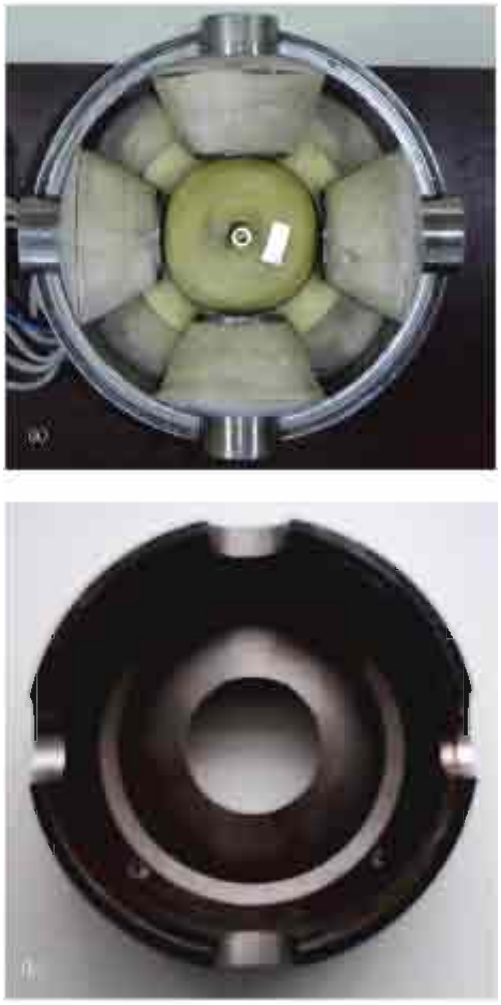

Fig. 1: (a) Internal view of the prototype and (b) End cap

The simulational and experimental investigations of the electromagnetic field distribution are one of critical topics for developing electromagnetic products. It provides a powerful tool to understand the distribution of a magnetic field which is an indispensable element to create the force/torque of these actuators. It can be used for verify the analytical or numerical result of a magnetic field as well as benefit the design optimization of products (Yan *et al*., 2005). In this study, a dc type of spherical permanent magnet motor is firstly modeled, simulated and optimized with a commercial software package (Ansoft Maxwell 3D); then, a prototype of this spherical motor is realized. The prototyped spherical motor offers the ability to spin continuously while the shaft is tilted arbitrarily up to ±45° from the Z-axis. The spherical motor comprises a system with a spherical moving part (rotor) with 4-pole permanent magnet, involved by a spherical surface (stator) made from soft-iron, having a uniform gap between them. The support mechanism (or bearing), produced from non-magnetic teflon material and preventing radial movement of the moving part due to electromagnetic attraction, is positioned to the air-gap. Some papers examining similar motor structures exist in the literature. Internal view of the prototype and end cap is shown in Fig. 1.

DESIGN OF PROTOTYPE

The spherical motor dealt with has been made up of three basic assemblies: a spherical rotor, a hallow spherical stator and end cap and a spherical bearing. The stator carries eight electromagnets strategically positioned on the spherical surface. A magnetic field is generated when an electric current flows through the stator poles. A magnetic attraction or repulsion is generated between the stator poles and the permanent-magnet-rotor poles as the electromagnetic system tries to reduce the reluctance along the magnetic path. The tangential component of the magnetic attraction or repulsion causes the rotor to rotate.

Design of rotor: The rotor does not need electric supply due to use of permanent magnets. The spherical rotor consists of four-pole spherical permanent magnets, which is formed with two pairs of parallel magnetized quarter-spheres. In Maxwell 3D model, the rotor is modeled as a perfect sphere; but it is realized by stacking of various sizes of four-pole cylindrical magnets in the prototype due to incapacities. After shaped by using five-cylindrical magnet, the rotor is coated with a teflon surface having a low friction constant. Neodymium-iron-boron (NdFeB) is chosen as permanent magnet material because of possessing higher specific energy density and better temperature stability. Remanent field density and relative permeability of NdFeB magnet used in the prototype are $B_r = 1.234T$, $\mu_r = 1.15$. The diameter of the rotor is decided at 60 mm (Fig. 2).

Design of bearing system: Another important part of the spherical motor being taken into consideration is the bearing system. In the history of spherical motor, a lot of spherical motor bearing systems or support mechanism was presented (universal mechanical wheel, off-centered wheel, carrying ball, spherical ball bearing, magnetic bearing, aerostatic bearing, etc.). Each solution, for a given size, has a different load capacity, allows different air-gap thickness (Dehez *et al*., 2005). The air-gap must be as small as possible in order to reduce the flux leakage. In

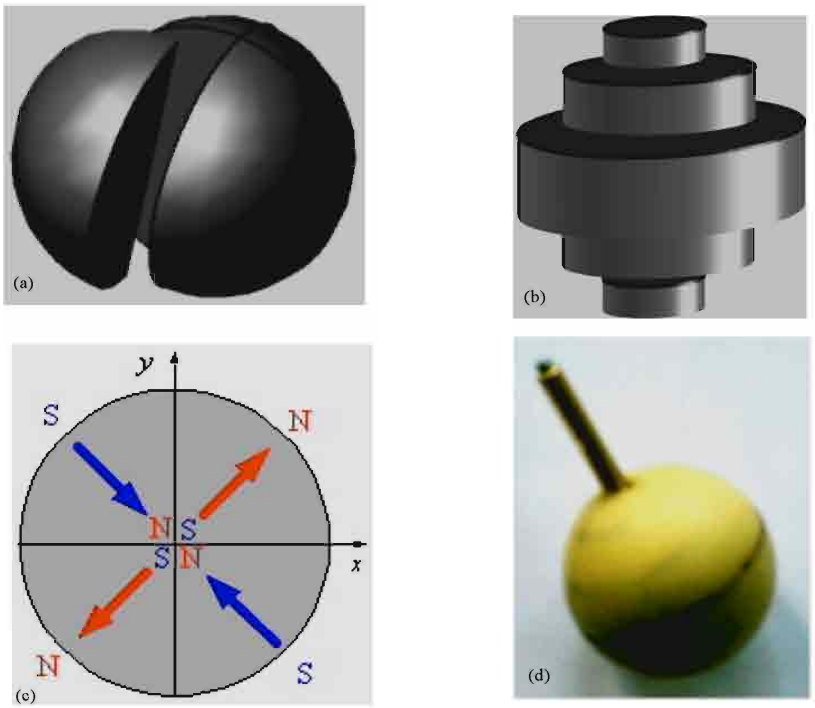

Fig. 2: The structural views of the rotor, a) Ansoft Maxwell 3D model, b) Experimental model, c) the direction of magnetic fields, d) prototype of the rotor

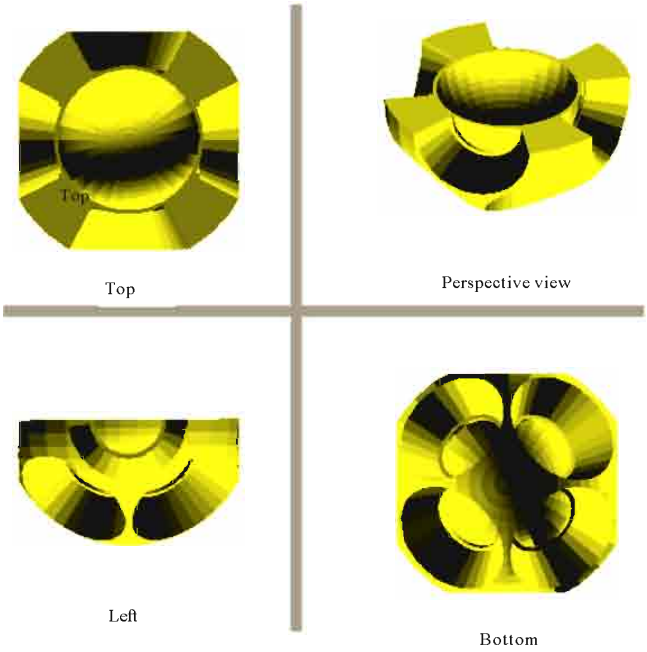

Fig. 3: Schematic of the bearing used in the prototype

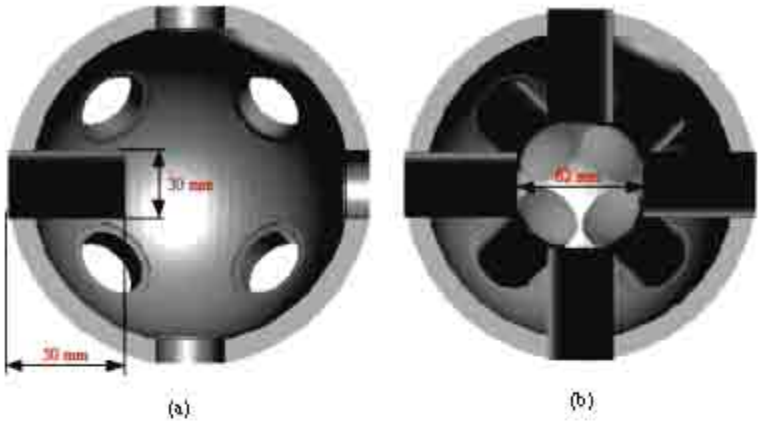

Fig. 4: (a) The stator structure and (b) Stator with eight-iron core of the coils

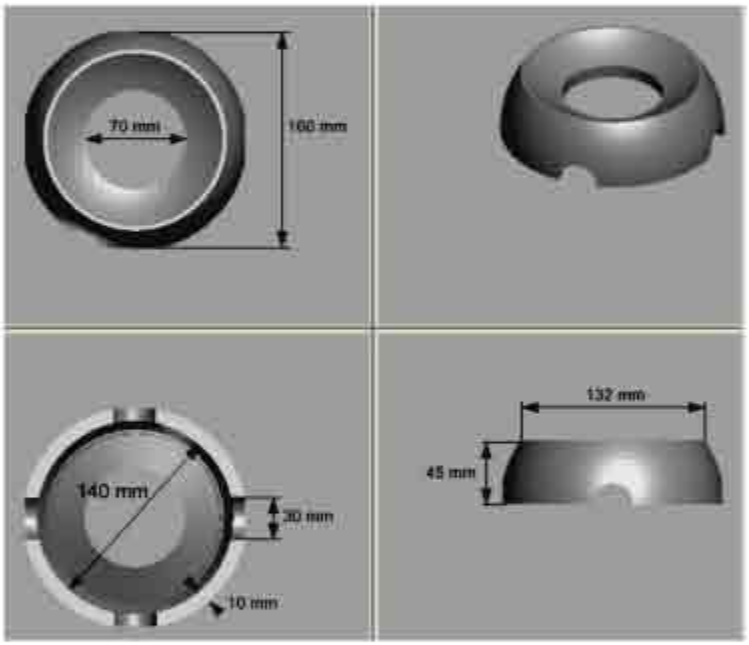

Fig. 5: Dimensions and perspective view of the stator end cap

our prototype, a different spherical bearing is used. The bearing is produced from a hollow semi-spherical teflon material with low density and non-magnetic properties and is positioned the air-gap between the rotor and the stator (Oner, 2004). We chose a bearing thickness of 0.2 mm at pole face of the coils and 12 mm elsewhere. The rotor is positioned in this hallow semi-spherical bearing. Thus, there is no need to center the rotor. Obviously, this type of bearing system has the drawbacks of high friction. But, high friction is minimized with a lubricant (Fig. 3).

Design of stator and end cap: The stator as shown in Fig. 4 not only houses the rotor but also serves the function of a fixture for positioning of the stator poles. Attraction force between rotor and stator poles forms the basis for motion generation. By impressing independent dc current in each of the appropriate coil and/or coils, a resultant magnetic field pointing to a radial direction in a 3D space occurs. The rotor is then subjected to a torque and moves to align its magnetic field with the resultant field produced by stator coils. In this way, it is possible to control rotor position by controlling the stator current

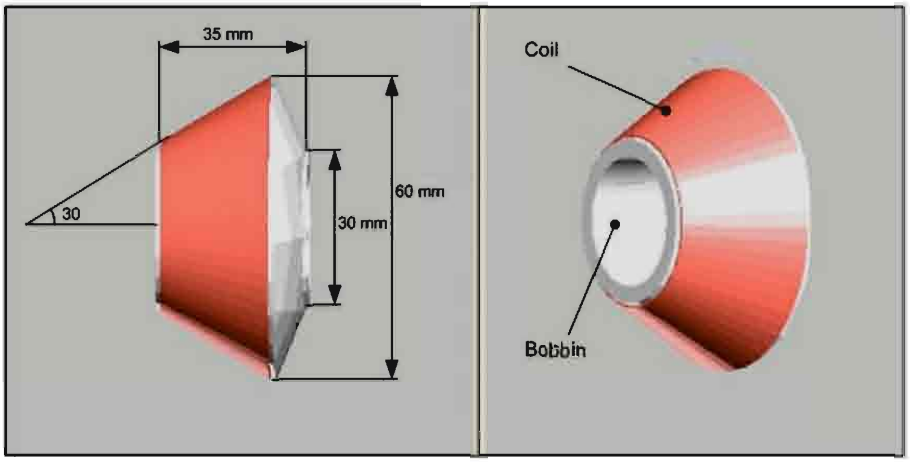

Fig. 6: Dimensions of the stator coils

value and stator current direction. The body of the stator (core) is produced from soft-iron. The main drawbacks of using ferromagnetic materials as core for the stator pole are the potentially large detent force and induced eddy current. However, without a high permeability core, one must have more and larger turns to achieve a given inductance value. More turns means larger coils, lower self-resonance and higher copper losses. These are factors that compromise the achievable dynamics performance of the spherical motor. External diameter of the stator is chosen as 160 mm and internal diameter of that is 140 mm.

The end cap is also produced from soft-iron. Thus, the flux linkage is increased. In addition to this, duties of the end cap include preventing the rotor movements in z-direction and protecting the internal parts of the stator from external influences (Fig. 5).

Design of coil: The eight iron-cored stator coils are arranged in such a way that three independently controllable torque components can be developed by energizing the appropriate coils. Four coils are evenly distributed along the equator of the stator. The other four coils are also evenly located at 45° apart from equator plane of the stator, but rotated 45°. Geometrically, the coils are materialized as a hollow cone. Thus, the maximum number of turns is attainable with the coil frame. Electromagnet wires with a diameter of 0.5 mm are used as the winding material of the stator coil. Number of turns of the coils is chosen as 1000. The pole faces of the coil's core are scooped out suitably in order to surround the rotor completely. Dimensions of the coil frame are given in Fig. 6.

MAGNETIC FIELDS DISTRIBUTION

This section presents the numerical computation of the magnetic field distribution. A knowledge of the magnetic field distribution produced by the spherical permanent magnet rotor is fundamental to establishing an accurate model of the motor, for design optimization and dynamic modeling (Wang *et al*., 1998, 2001). Without loss of generality, an air-cored motor is considered. Thus, the entire magnetic field region can be divided into two sub-regions, the outer airspace/winding region in which the permeability is μ_0 and the magnet region in which the permeability is $\mu_0\mu_r$. Therefore,

$$B = \begin{cases} \mu_0 H \\ \mu_0\mu_r H + \mu_0 M \end{cases} \quad (1)$$

Where:
μ_r = The relative recoil permeability of the magnet.
M = Its remanent magnetization.

For a permanent magnet having a linear magnetization characteristic, μ_r is constant and M is related to the remanence, Brem, by $M = B_{rem}/\mu_0$. It is convenient to formulate the field distribution in terms of a scalar potential φ, defined as $H = -\nabla\varphi$ and the spherical co-ordinate system shown in Fig. 7. This leads to the following field equations:

$$\begin{cases} \nabla^2\varphi_I = 0 \\ \nabla^2\varphi_{II} = \nabla.M/\mu_r \end{cases} \quad (2)$$

The radial components M_r may be expanded into spherical harmonics of the following form:

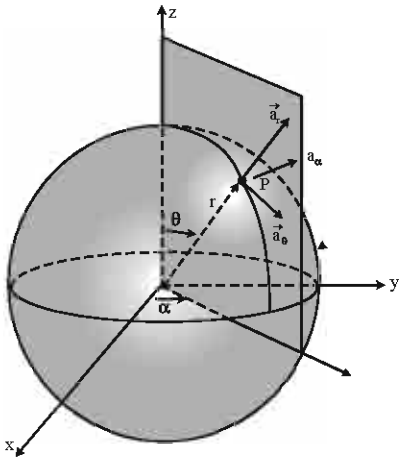

Fig. 7: Orientation angles defined in spherical co-ordinate system

$$M_r = \sum_{l=2,4,}^{\infty} \sum_{m=1,3,}^{l} M_{lm} P_l^m(\cos\theta)(\sin\alpha) \quad (3)$$

Where, P_l^m denotes the associated Legendre polynomial of degree *l* and order m and M_{lm} given by:

$$M_{lm} = \frac{4(2l+1)(l-m)!}{\pi m(l+m)!} M_c \int_0^1 P_l^m(x)\, x\, dx \quad (4)$$

Where, $M_c = B_{rem}/\mu_0\sqrt{2}$ Solving for Eq. 2 with boundary conditions yields following expression for the flux density distribution in the airspace/winding region (Wang *et al*., 2001):

$$B_{lr} = \sum_{l=2,4,}^{\infty} \sum_{m=1,3,}^{l} C_{lm}(l+1) r^{-(l+2)} P_l^m(\cos\theta)(\sin\alpha) \quad (5)$$

$$B_{l\theta} = \sum_{l=2,4,}^{\infty} \sum_{m=1,3,}^{l} C_{lm} r^{-(l+2)} \frac{d}{d\theta} P_l^m(\cos\theta)(\sin\alpha) \quad (6)$$

$$B_{l\alpha} = \sum_{l=2,4,}^{\infty} \sum_{m=1,3,}^{l} \frac{mC_{lm}}{\sin\theta} r^{-(l+2)} \frac{d}{d\theta} P_l^m(\cos\theta)(\cos\alpha) \quad (7)$$

Where, C_{lm} is given by:

$$C_{lm} = -\mu_0 R_m^{l+2} M_{lm} / [(l+l(l+\mu_r)] \quad (8)$$

Bu using the equations given above, analytical results of radial component of flux density as a function of α and θ are computed with Mathematica® and then expressed in 3D space (Fig. 8).

Fig. 8: Analytical results of radial component of flux density as a function of α and θ

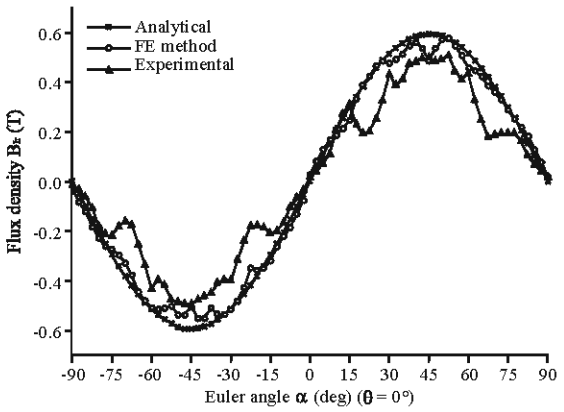

Fig. 9: Radial component of flux density as a function of Euler angle α (θ = 0°)

This analytical result has been validated by Finite Element (FE) analysis and experimental study. The results of both FE analysis and experimental study are normalized with the analytical results. Figure 9 shows of the finite analysis, analytical and experimental results under these conditions: $R_m = 0.030$ m, r = 0.031 m, θ = 0°, -90° ≤α≤ 90°. The differences between analytical solution and finite element analysis result from the effect of discreatization in the finite element model. The deviations in experimental study arise from stacking of various sizes of NdFeB magnets in order to form the spherical rotor.

Photograph of the experimental setup from which the experimental results are taken is given in Fig. 10. The rotor carries an electronic camera as its payload. A PIC16F877 microcontroller with 4MHz oscillator is used for controlling the spherical motor. Torque values are measured with the sensor of Alpha Load Beam produced by BLH electronics.

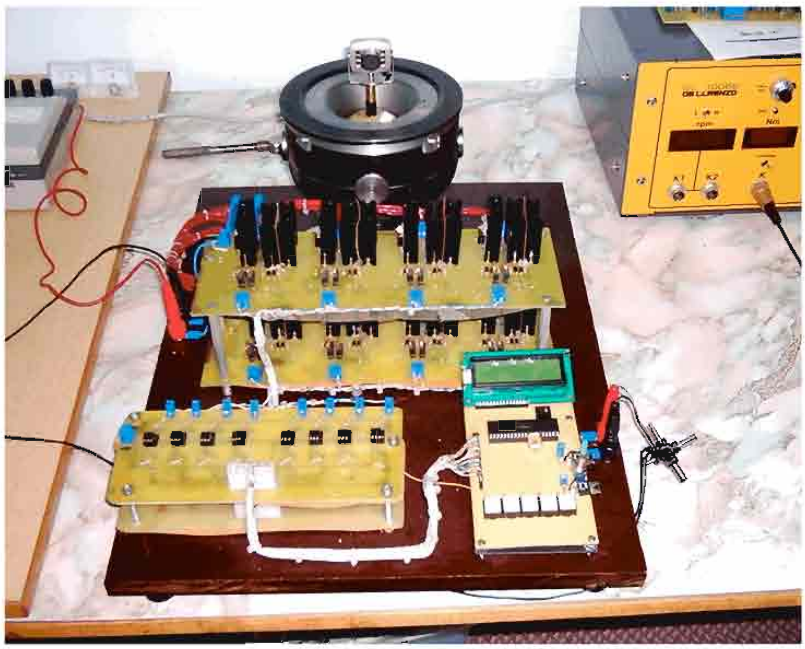

Fig. 10: Experimental setup

3D ANALYSIS OF THE MAGNETIC FIELDS

The three dimensional structure of the electromagnetic field distribution in almost all proposed spherical motors makes their electromagnetic and dynamic behavior difficult to analyze and this difficulty is a significant obstacle to their design optimization and servo application.

When a new mechanism is developed or a system is formulated, it is often convenient to study the system performance by simulation before building the breadboard or prototype. The simulation not only validates the system's performance, but also permits optimization of the system's performance by iteration of its parameters. Thus, valuable time saved in the development and design of a product and the failure of components of poorly designed system can be avoided.

In this study Ansoft Maxwell 3D, a commercial software package using FE method, is utilized in the computation of torques. For ideal analysis of the prototype and the computation of torque, a full three-dimensional (3D) model is necessary. Therefore, 3D solid model of the spherical motor is firstly created. Then, to perform FE analysis in Ansoft Maxwell 3D, each part is assigned appropriate element type along with the material property before being meshed. FE model is completed by enclosing the rotor and stator with a volume of air and then, the model is meshed to 250000 elements. The torque produced from the magnetic fields is calculated with the software by rotating the rotor with an α angle interval of 5° and a θ angle interval of 10°. Thus, a total of 648-static-magnetic analysis is performed. For the rotor assembly, NdFe38 elements are used as permanent magnet materials in the program. For free space air region, the relative permeability of $\mu_r = 1$ is assigned. We model the stator coils as a cylindrical iron-cored electromagnets. The relative permeability of $\mu_r = 1000$ is chosen for all ferromagnetic materials used in the spherical motor. As an example, flux densities/linkages of the spherical motor obtained from magnetostatic analysis for $\theta = 0°$, $\alpha = 30°$ is shown in Fig. 11. In according to this analysis, it can be seen that the flux densities at the pole surface (coil's cores) become different; the flux density has a tendency to increase at counter-clockwise and it has a tendency to decrease at clockwise, which means that the spherical motor is generating a torque.

The magnetic field distribution is required to evaluate the generated torque. The torque of an electromagnetic actuator is a function of magnetic field distribution governed by Maxwell's equations. Maxwell's equations are formulated into Poisson equation either by the vector potential method or scalar potential method. In the Ansoft Maxwell 3D, the maxwell equations are solved by using the scalar potential formulation. The virtual work method is used to calculate the force distribution on the rotor.

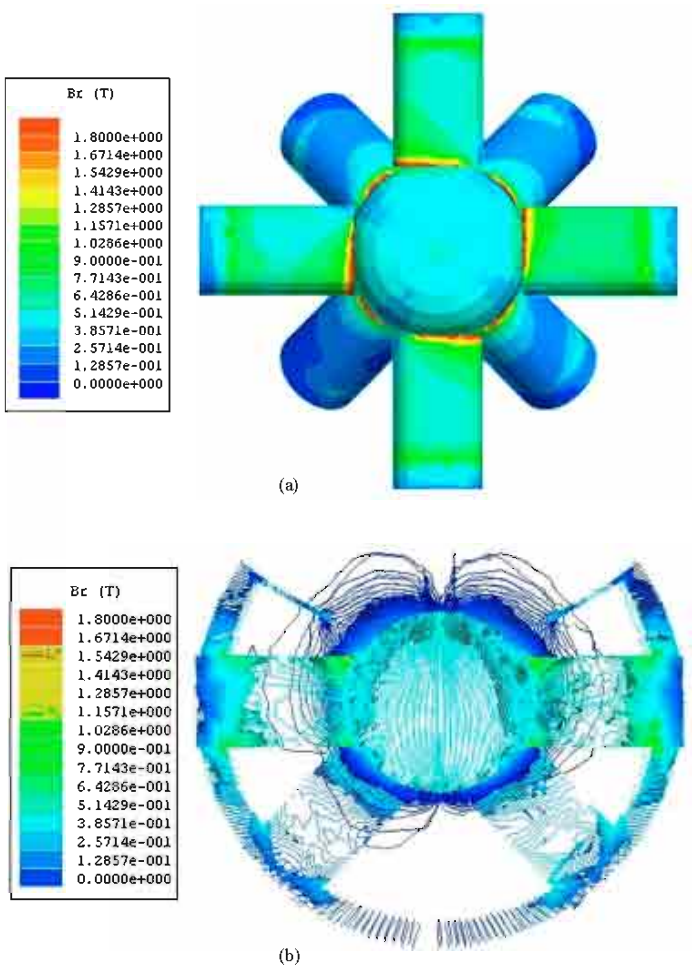

Fig. 11: Magnetostatic analysis of the spherical motor ($\theta = 0°$, $\alpha = 30°$), a) Flux densities (top view), b) Fluxlinkages at cross-section of yz-plane

SIMULATION AND EXPERIMENTAL RESULTS

Visualization of the calculated results aids in understanding the design procedure. In spherical co-ordinate systems a point can be represented one set of three parameters (α, θ, r). By using the torque values T in place of r and by varying α and θ in hardware limits ($\alpha = [-\pi: \pi]$, $\theta = [-\pi/4:\pi/4]$), the values of the torque have been introduced in a 3D space as a surface in cartesian co-ordinate systems (Fig. 12). Based on this visualization, a prototype design has been carried out. In according to Fig. 12, the rotor torque along the α direction has eight positive/negative peaks. This event is caused by the eight alternately energized electromagnets on the stator. In contrast, the torque declines gradually in θ direction because of the rotor and stator structures.

Torque graphics are not sinusoidal and positive and negative peak values are not also equal. This result from manufacturing tolerances and the rotor structure which is not a perfect sphere (Fig. 12).

Using polar co-ordinates, angle-dependent data can be displayed quickly and easily. This is also very illustrative for spherical motor making angle-dependent movements (Fig. 13).

In the experimental setup, the SM control system contains a control board, a power supply, one motor-interface board and a set of sensors. The rotor position of the SM has been controlled with a micro-controller-unit. In order to keep the design as simple and cheap we have chosen PIC16F877 as a micro-controller-unit offering up to 20MHz clock frequency, eight ADC channels with

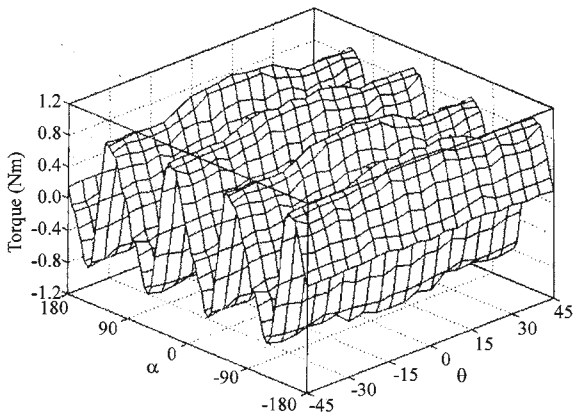

Fig. 12: The torque values displayed in 3D space

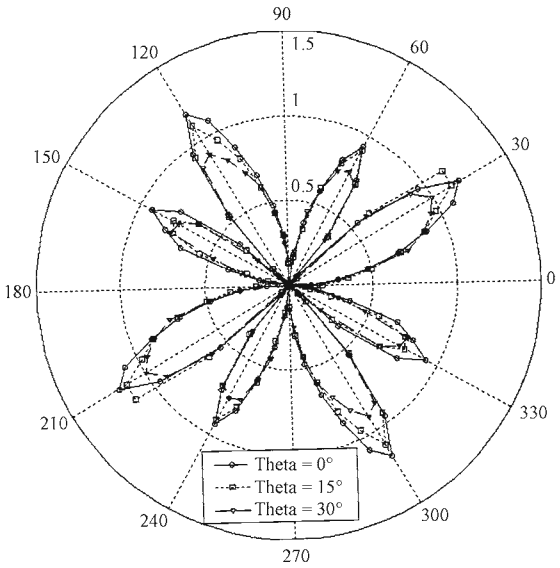

Fig. 13: The torque values displayed in polar graphics

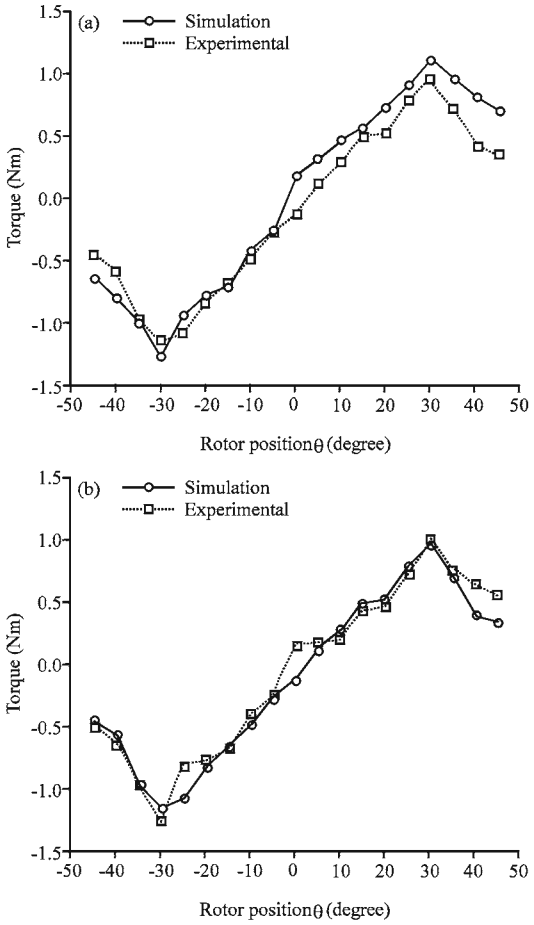

Fig. 14: (a) Torque values in the direction of x-axis ($\alpha = 0°$, $\theta = \pm 45°$) and (b) Torque values in the direction of y-axis ($\alpha = 0°$, $\theta = \pm 45°$)

10-bit, 8K×14 words of FLASH program memory, 256×8 bytes of EEPROM data memory, two CCP modules and thirteen I/O ports. To illustrate the performance of the described SM, a laboratory test was constructed. The experimental work is carried out with the input stator currents of 0.2A, 0.4A, 0.6A, 0.8A and 1A. The torque produced from the SM is measured with a torque sensor (BLH-Alpha Load Beam). Experimental and simulation results at the stator current of 1A are shown in Fig. 14. Figure 14a shows alteration of the torque in the direction of x-axis and Fig. 14b shows alteration of the torque in the direction of y-axis. The agreement between experimental and simulation results is satisfactory and the discrepancy is attributed to two main factors. The first is due to the mechanical losses including friction, windage and etc. The second is due to the structure of the spherical rotor which is realized by stacking of various sizes of four-pole cylindrical magnets. Other ineffective factors for disagreement are due to the iron losses and the finite element mesh. The 3D-model obtained using FE method offers more insight and accurate representation of torque generated by a spherical motor, which is essential for both design optimization and control of the spherical motor. The capabilities offered by the ANSOFT finite element formulation of the spherical motor could, therefore, lead to a significant reduction in the design cycle time (Oner, 2004).

CONCLUSIONS

In this study, a dc version of three-DOF permanent-magnet spherical motor has been modeled and analyzed with a commercial software package (Ansoft Maxwell 3D)

and the torque values have been computed by the software package using FE method and then a prototype of the modeled spherical motor is realized. Experimental test revealed that this prototype could achieve a torque of 1.15 N m with a pan and tilt excursion of ±45°. Maximum speed of the spherical motor is 541 rpm (56.65 rad sec^{-1}). In addition, after the data processing, electromagnetic torques obtained from the software are plotted within the 3D space and polar graphics for better visualization, which facilitates the observation and analysis of the design greatly. The main drawback in this design lies in the bearing mechanism. The direct contact between rotor and bearing system reduces the generated torque. The friction loss can be minimized with a lubricant.

REFERENCES

Davey, K., G.J. Vachtsevanos and R. Power, 1987. An analysis of fields and torques in spherical induction motors. IEEE Trans. Magn. Mag., 23: 273-281.

Dehez, B., V. Froidmont, D. Grenier and B. Raucent, 2005. Design, modeling and first experimentation of a two-degree-of-freedom spherical actuator. Robo. Comput. Integr. Manufact., 21: 197-204.

Foggia, A., E. Oliver and F. Chappuis, 1988. New three degree of freedom electromagnetic actuator. Conference Record IAS Annual Meeting 35, New York.

Hollis, R.L. and L. Ralph, 1989. Magnetically Levitated Fine Motion Robot Wrist with Programmable Compliance. United States Patent, October.

Kaneko, K., I. Yamada and K. Itao, 1989. A spherical DC servo motor with three degrees of freedom. Trans. ASME J. Dyn. Syst. Measur. Control, 111: 398-402.

Lee, K.M. and C. Kwan, 1991. Design concept development of a spherical stepper for robotic applications. IEEE Trans. Robot. Auto., 1: 175-181.

Lee, K.M., Z. Wei and J. Joni, 2004. Parametric study on pole geometry and thermal effects of a VRSM. Conference on Robotics, Automation and Mechatronics. Proceeding IEEE, pp: 548-553.

Lim, C.K., L. Yan and I.M. Chen *et al*., 2004. Mechanical design and numerical electromagnetic analysis of a dc spherical actuator. Conference on Robotics. Automation and Mechatronics. Proceeding IEEE, pp: 536-541.

Lim, C.K., I.M. Chen and L. Yan *et al*., 2005. Design and Analysis of a new variable stator pole for a DC spherical Actuator. International Conference on Advanced Intelligent Mechatronics. Proceeding IEEE/ASME, pp: 341-346.

Oner, Y., 2004. Computer aided three dimensional magnetic analysis, design and application of a permanent magnet spherical motor. Ph.D Thesis, Institute of Science and Technology, Gazi University.

Roth, R. and K.M. Lee, 1995. Design optimization of a three degrees of freedom variable reluctance spherical wrist motor. Trans. ASME J. Eng. Ind., 117: 378-388.

Shigeki, T., Z. Guoqiang and M. Osamu, 1996. Development of new generation spherical ultrasonic motor. International Conference on Robotics and Automation. Proceeding IEEE, pp: 2871-2876.

Wang, J., W. Weiya, G.W. Jewell and D. Howe, 1998. A novel spherical permanent magnet actuator with three degrees of freedom. IEEE Trans. Magne., 34: 2078-2080.

Wang, J., K. Mitchell, G.W. Jewell and D. Howe, 2001. Multi-degree-of-freedom spherical permanent magnet motors. International Conference on Robotics and Automation. Proceeding IEEE, pp: 1798-1805.

Yan, L., I.M. Chen and C.K. Lim *et al*., 2005. Experimental investigation on the magnetic field of a permanent magnet spherical actuator. Int. Con. Advanced Intelligent Mechatronics. Proceeding of the IEEE/ASME, pp: 347-352.

Zhao, C., Z. Li and W. Huang, 2005. Optimal design of the stator of a three-DOF ultrasonic motor. Sensors and Actuators A, 121: 494-499.

Zhou, Z. and K.M. Lee, 1996. Real time motion control of multi degree of freedom variable reluctance spherical motor. Proceedings of the 1996 IEEE International Conference on Robotics and Automation, pp: 2859-2864.